

Submitted to the Astrophysical Journal (Letters)

## A Compact X-ray Source and Possible X-ray Jets within the Planetary Nebula Menzel 3

Joel H. Kastner<sup>1</sup>, Bruce Balick<sup>2</sup>, Eric G. Blackman<sup>3</sup>, Adam Frank<sup>3</sup>, Noam Soker<sup>4</sup>, Saeqa D. Vrtilík<sup>5</sup>, and Jingqiang Li<sup>1</sup>

### ABSTRACT

We report the discovery, by the Chandra X-ray Observatory, of X-ray emission from the bipolar planetary nebula Menzel 3. In Chandra CCD imaging, Mz 3 displays hot ( $\sim 3 - 6 \times 10^6$  K) gas within its twin, coaxial bubbles of optical nebulosity, as well as a compact X-ray source at the position of its central star(s). The brightest diffuse X-ray emission lies along the polar axis of the optical nebula, suggesting a jet-like configuration. The observed combination of an X-ray-emitting point source and possible X-ray jet(s) is consistent with models in which accretion disks and, potentially, magnetic fields shape bipolar planetary nebulae via the generation of fast, collimated outflows.

*Subject headings:* stars: AGB and post-AGB — stars: mass loss — stars: winds, outflows — ISM: jets and outflows — planetary nebulae: individual (Menzel 3)

### 1. Introduction

Planetary nebulae (PNs) are the descendents of intermediate-mass stars (initial masses  $\sim 1 - 8M_{\odot}$ ). The central star of a PN eventually will evolve into a white dwarf, with a

---

<sup>1</sup>Chester F. Carlson Center for Imaging Science, Rochester Institute of Technology, Rochester, NY 14623; jhk@cis.rit.edu

<sup>2</sup>Department of Astronomy, University of Washington, Box 351580, Seattle, WA 98195, USA; balick@astro.washington.edu

<sup>3</sup>Department of Physics and Astronomy, University of Rochester, Rochester, NY 14627, USA

<sup>4</sup>Department of Physics, Oranim, Tivon 36006, Israel; soker@physics.technion.ac.il

<sup>5</sup>Harvard-Smithsonian Center for Astrophysics, Cambridge, MA 02138, USA; saku@cfa.harvard.edu

mass of between  $\sim 0.55M_{\odot}$  and  $\sim 1.0M_{\odot}$ . Much of the star’s initial mass is expelled during the  $\sim 10^5$  years that the star spends on the upper asymptotic giant branch (AGB). This AGB star wind usually consists of a more or less spherically symmetric outflow at rates of up to  $10^{-4} M_{\odot} \text{ yr}^{-1}$  and speeds of  $\sim 10 - 20 \text{ km s}^{-1}$ . As the star leaves the AGB, however, its surface escape velocity and, hence, wind speed, drastically increases to  $\sim 1000 \text{ km s}^{-1}$  and its mass loss rate drops to  $10^{-8} M_{\odot} \text{ yr}^{-1}$ . Eventually, the UV flux from this emerging white dwarf ionizes the AGB ejecta, producing a PN detectable in atomic recombination line emission.

Optical images of PNs obtained by the Hubble Space Telescope (HST) very clearly show that, during late AGB and/or early PN stages, the geometry of the outflow often takes on axial (bipolar) or even more spectacular, high-order symmetries (Sahai & Trauger 1998; Kastner, Soker & Rappaport 2000a; Balick & Frank 2002). Various models have been proposed to explain this transition; some or all of these may apply at different times and to various central star configurations. For example, during late AGB phases when the mass loss rate is highest, the accretion of material by a nearby companion may cause a collimating disk to form (Mastrodemos & Morris 1999; Soker & Rappaport 2000; and references therein). The presence of such a companion and disk potentially provides an additional source of wind momentum and/or ionizing UV flux, thereby significantly altering the “standard” picture of late-AGB, early-PN evolution described above. Another proposal is that magnetic fields emerge from the stellar core as the AGB star’s outer layers are stripped away (Blackman et al. 2001b). The resulting  $\sim 1 \text{ G}$  fields can either help to collimate the radiation driven wind, or mediate a stronger, more anisotropic, magnetically driven wind. This stellar wind can interact with, and be collimated by, a surrounding magnetically mediated disk wind. Disk winds and stellar winds may therefore operate in tandem to produce the observed rates and morphologies of mass loss and very high momenta of outflowing material prior to the onset of wind ionization by the emerging white dwarf (Blackman et al. 2001a, Frank et al. 2003).

The tenuous but very fast stellar wind from the emerging central white dwarf (or a companion, if the mass-losing central star is still on the AGB) will shock the relatively slow-moving AGB ejecta, creating an overpressured (and therefore rapidly expanding) “hot bubble” interior to the optical nebula. The shocked gas generated by these PN wind interactions should be detectable in the form of X-ray emission that fills an optically dark cavity within swept-up stellar ejecta. Simple energy conservation arguments predict that such a wind-heated bubble can reach temperatures of  $10^7 - 10^8 \text{ K}$ , although it is likely that the bulk of the shocked gas will appear cooler ( $\sim 10^6 \text{ K}$ ), due to various processes (such as early wind onset, adiabatic expansion, and conduction of heat from the wind-shocked gas to cooler, denser nebular gas) that can moderate the gas temperature (Soker & Kastner 2003a, and references therein). In addition, the new classes of PN shaping models that rely on mag-

netohydrodynamics and/or the presence of accreting, magnetically active companion stars predict magnetic fields at the base of the flow that are strong enough to produce detectable, compact X-ray emission (Blackman et al. 2001a; Soker & Kastner 2002). Hence, there is reason to expect both point-like and diffuse X-ray emission from some PNs.

Correspondingly, recent observations by the Chandra X-ray Observatory (CXO) and XMM-Newton have revealed examples of diffuse, X-ray-emitting gas within the well-studied PNs BD +30°3639 (Kastner et al. 2000b), NGC 7027 (Kastner, Vrtílek & Soker 2001), and NGC 7009 (Guerrero et al. 2002), point-like emission within NGC 7293 (Guerrero et al. 2001), and both diffuse and point-like emission within NGC 6543 (Chu et al. 2001; Guerrero et al. 2001). In optical and infrared images, all four PNe thus far detected in diffuse X-ray emission share a general elliptical morphology, punctuated by knots or loops indicative of recently established, high-velocity, collimated flows. In this *Letter* we extend the high-resolution X-ray observations to the important class of extreme bipolar PNe (referred to as “butterfly” PNs; Balick & Frank 2002), via CXO observations of Menzel 3 (Mz 3 = Hen 2-154 = PK 331-01 1 = PN G331.7-01.0).

Mz 3 has long been considered a prototypical example of an extreme bipolar PN (López & Meaburn 1983). Like many objects in this class, however, the core of Mz 3 is evidently a symbiotic Mira system, consisting of an AGB primary with dense, slow winds and a companion white dwarf that provides the UV flux which ionizes the nebula. The symbiotic Mira nature of Mz 3 is revealed by deep optical spectra (Zhang & Liu 2002) and by infrared colors (Schmeja & Kimeswenger 2001). If Mz 3 is indeed a symbiotic system, then it may not be a PN, but rather a PN in the making; nevertheless, we refer to it as a PN in this paper.

In high-resolution, visual-wavelength images obtained by the HST, Mz 3 presents a highly complex morphology (Fig. 1). Its bright, bipolar lobes appear as enclosed bubbles embedded within a larger cylindrical structure; this structure is in turn surrounded by an extended set of “streamers” that seem to point directly away from the central star. The distance to Mz 3 is poorly known (Zhang & Liu 2002) but, adopting an estimate of 2.7 kpc (Kingsburgh & English 1992), each enclosed bipolar bubble is  $\sim 40,000$  AU long.

High-resolution optical spectroscopy reveals that gas in Mz 3 is outflowing along its polar axis at velocities of between  $300 \text{ km s}^{-1}$  and  $500 \text{ km s}^{-1}$  (Redman et al. 2000; Balick, unpublished; Guerrero et al. 2003). Such velocities are only observed, for PNe, in the case of the most extreme bipolar objects (Bujarrabal et al. 2001). The potential for X-ray-generating shocks due to the collimated, fast winds in Mz 3, and the evidence that it harbors a central binary system, makes this nebula a particularly interesting object to probe for X-ray emission at high resolution.

## 2. Observations

We observed Mz 3 with Chandra for 40.83 ks on 2002 October 23. The detector was the back-illuminated CCD S3 of the Advanced CCD Imaging Spectrometer (ACIS). ACIS has a pixel size of  $0.49''$  — very similar to the width of the point spread function (PSF) of the Chandra mirrors — and the Chandra/ACIS combination is sensitive over the energy range 0.3-10 keV. The data, consisting of individual CCD X-ray and particle events, were subject to standard processing by Chandra X-ray Center pipeline software (CIAO<sup>6</sup>, version 2.2), which determines the distribution of photon-generated charge within a  $3\times 3$  CCD pixel island centered on the event position, flags events likely due to particles, and computes the celestial positions and nominal energies of incident X-rays. To optimize image resolution, the event charge distributions were used, along with the telescope pointing history and nominal photon energies, to calculate a subpixel position for each X-ray (Li et al. 2003).

## 3. Results

The Chandra/ACIS-S3 image of Mz 3 (Fig. 1) represents the first detection of X-rays from this object. Both diffuse and point-like X-ray emission is detected. The central X-ray source lies at the position of the central star seen in HST images, based on the spatial coincidence of several background HST sources with X-ray sources in the Chandra/ACIS-S3 field.

We used CIAO tools (version 2.3) to extract X-ray source counts and spectra within  $7.5'' \times 19''$  elliptical and  $3.5''$  diameter regions encompassing the diffuse and point-like emission, respectively. We find a total, background-subtracted count rate of  $1.9 \pm 0.2 \text{ ks}^{-1}$  (0.2 – 2.5 keV) from the combined diffuse and point-like components. We estimate that  $\sim 60$  total counts arise from the diffuse emission, and  $\sim 17$  from the central source.

Nearly all of the detected emission from Mz 3 is confined to energies between 0.6 and 2.0 keV (Fig. 2). Its X-ray spectral distribution is similar to that of NGC 7027, indicative of an X-ray emission temperature in the range  $3 - 8 \times 10^6 \text{ K}$  (Kastner et al. 2001; Maness et al. 2003). To confirm this, we used CIAO spectral fitting tools to perform fits of a variable-abundance thermal emission (VMEKAL) model with intervening absorption. Results from optical spectroscopy (Zhang & Liu 2002, their Table 11) were used to constrain the model abundances. Adopting these abundances, we find an X-ray emission temperature of  $T_x = 6 \times 10^6 \text{ K}$  and absorbing column of  $N_H = 5 \times 10^{21} \text{ cm}^{-2}$ . Because the observed spectral energy

---

<sup>6</sup><http://cxc.harvard.edu/ciao/>

distribution is sharply peaked, the formal uncertainties in these parameters are  $\sim \pm 15\%$ , despite the poor photon counting statistics. Given the likelihood that the abundances of the X-ray-emitting gas depart significantly from the nebular abundances (e.g., Chu et al. 2001; Maness et al. 2003), however,  $T_x$  and  $N_H$  are actually not so well constrained, and the model fitting procedure cannot be used to further refine abundances for the X-ray emitting region (in contrast to results in, e.g., Maness et al.). In particular, although the best-fit model abundances of Ne and Fe — 0.4 and 0.2 solar, respectively — appear consistent with the nebular values (0.4 and 0.3 solar, respectively; Zhang & Liu), each is uncertain by a factor  $\sim 3$ , reflecting the uncertainty in assigning the emission peak near 0.9 keV to highly ionized Ne, highly ionized Fe, or both. If Fe is severely depleted (as appears to be the case for BD +30° 3639; Maness et al. 2003), we find that values of  $T_x \sim 3 \times 10^6$  K and  $N_H \sim 8 \times 10^{21}$  cm $^{-2}$  provide the best fit.

Adopting values of  $T_x = 6 \times 10^6$  K and  $N_H = 5 \times 10^{21}$  cm $^{-2}$ , the absorbed flux derived from the model fitting procedure is  $7 \times 10^{-15}$  erg cm $^{-2}$  s $^{-1}$ . The implied total (combined diffuse and point-like) intrinsic source X-ray luminosity is  $\sim 3 \times 10^{31} (\frac{D}{2.7\text{kpc}})^2$  erg s $^{-1}$ , where  $\sim 6 \times 10^{30} (\frac{D}{2.7\text{kpc}})^2$  erg s $^{-1}$  can be ascribed to the point source under the assumption that its intrinsic spectrum is not much harder than that of the diffuse component (see below).

As in previous X-ray detections of PNs, the modeling results for intervening X-ray absorbing column are consistent with measurements of visual extinction. Zhang & Liu (2002) deduce  $E(B - V) = 1.38$  and  $E(B - V) = 1.59$  toward the nebula and the central star, respectively, suggesting  $A_V \approx 4.5$ . Hence, the ratio  $N_H/A_V$  in Mz 3 ( $\sim 10^{21}$  cm $^{-2}$  mag $^{-1}$ ) is similar to that in BD +30°3639 and in NGC 7027 (Kastner et al. 2000b, 2001, 2002; Maness et al. 2003). There is probably a significant absorption component that is due to the interstellar medium along the line of sight to Mz 3, given its large estimated distance and low galactic latitude ( $b = -1.01^\circ$ ). The nebula is a strong far-infrared source (IRAS 25  $\mu\text{m}$  flux of 343 Jy) and displays a local component of diffuse optical absorption bands (Zhang & Liu), however, indicating that some or most of the soft X-ray absorption is due to dense gas and dust within the nebula itself.

## 4. Discussion

### 4.1. An X-ray jet and obscured central X-ray source in Mz 3

The CXO imaging reveals a strong correspondence between the diffuse X-ray emitting region of Mz 3 and its visual-wavelength emission (Fig. 3). Specifically, the diffuse X-ray emission is confined to the interiors of the bubbles of ionized gas seen in HST imaging. This

correspondence resembles those of earlier CXO and XMM-Newton detections of diffuse X-ray emission from planetaries (Kastner et al. 2000b, 2001, 2002; Chu et al. 2001; Guerrero et al. 2002). With the possible exception of NGC 7027 (Kastner et al. 2001, 2002), the X-ray emitting gas is precisely outlined by bright elliptical shells within these nebulae.

In contrast, the brightest X-ray emission from Mz 3 lies close to the symmetry axis of the object (Fig. 3). This morphology strongly suggests that most of the diffuse X-ray emission is associated with collimated outflows, perhaps in the form of jets. Jet-like structure is suggested by the diffuse emission south of the nucleus. In particular, there is a “knot” of emission located along the polar axis,  $\sim 11,000$  AU ( $4''$ ) south of the source. Based on the density of field X-ray sources within  $\sim 1'$  of Mz 3, we estimate that there is only a  $\sim 3\%$  probability that this feature is a foreground or background X-ray source. A plausible interpretation of the diffuse X-ray morphology within the south lobe of Mz 3, therefore, is that this lobe harbors a “blobby” X-ray jet that extends at least  $18,000$  AU ( $7''$ ) from the central source, perhaps terminating at the leading edge of the southern lobe.

To the north of the central star the X-ray and optical surface brightness distributions are somewhat more amorphous, with the X-ray emission brightest near the tip of, and apparently outlining, the protrusion in the north lobe. No feature corresponding to the southern X-ray “knot” is seen immediately to the north of the central star. Instead, there appears to be a gap within the diffuse X-ray nebula, spatially coincident with a similar feature in optical recombination line emission, just north of the central source. As high-resolution optical spectroscopic observations indicate that the north lobe is slightly tipped away from the observer (e.g., Redman et al. 2000), it is possible that the lack of emission just to the north of the central star is due to the orientation of the nebula, which is such that the inner northern lobe is partially obscured by material located along the equatorial plane. Alternatively, the X-ray emission along the polar axis of Mz 3 may be intrinsically asymmetric, as is the case in another symbiotic Mira system, R Aqr (Kellogg et al. 2001; see §4).

All of the photons detected from the central source have energies  $\geq 1$  keV, suggesting either that this source is intrinsically harder than the shocked nebular gas or, perhaps, that the central source is especially deeply embedded in X-ray absorbing gas. The latter interpretation is consistent with the relative degree of visual extinction, which is larger toward the central star than toward the nebula (Zhang & Liu 2002).

#### 4.2. The X-ray evidence for magnetized accretion disks in symbiotic Miras

The combination of an X-ray-bright core and X-ray emission along the polar axis of Mz 3 resembles that observed in R Aqr (Kellogg et al. 2001), which is also a symbiotic Mira system. Adopting respective distances of 2.7 kpc and 200 pc, however, the X-ray emission from Mz 3 appears much more luminous and extensive than that of R Aqr, which has a total X-ray luminosity  $\sim 10^{30}$  erg s $^{-1}$  and whose discontinuous, southwest jet (the longer of its two, asymmetric X-ray jets) extends  $\sim 6000$  AU from the central source. If, instead, Mz 3 is as close as  $\sim 1$  kpc — the smallest of many, disparate distance estimates for this PN (see Zhang & Liu 2002 and references therein) — the X-ray properties of this symbiotic Mira system and R Aqr would be remarkably similar.

Alternative explanations for the unresolved, core X-ray emission within Mz 3 and R Aqr (see also Guerrero et al. 2001 and Soker & Kastner 2002) are (1) magnetic star-disk interactions (or, perhaps, accretion shocks) associated with accretion by a companion to the central AGB star; (2) star-disk interactions or shocks due to accretion by the AGB star itself (if the secondary is less than a solar mass, and approaches close enough to the AGB star to be tidally disrupted; Reyes-Ruiz & López 1999); (3) stellar magnetic activity originating with the AGB star (e.g., Blackman et al. 2001a; García-Segura, López, & Franco 2003; Soker & Kastner 2003b); (4) X-ray-generating wind shocks analogous to those around O/B stars (e.g., Cassinelli et al. 1994); or, perhaps most speculatively, (5) hard X-ray emission from the companion white dwarf itself (e.g., O’Dwyer et al. 2003).

Given that both Mz 3 and R Aqr evidently harbor symbiotic binary central stars, it seems most likely that the compact X-ray source arises, in each case, from an accretion disk around a hot secondary (alternative 1, above). By analogy with, e.g., models for disk-driven winds from young stellar objects (YSOs), such a configuration also would explain the presence of high-velocity, collimated winds that generate X-rays as they collide with ambient nebular gas (e.g., Pravdo et al. 2001).

It has been proposed that magnetic fields play a fundamental, dynamical role in disk-jet systems as diverse as YSOs (e.g., Pudritz & Konigl 2000), active galactic nuclei (AGNs; e.g., Ferrari 1998 and references therein), and, indeed, R Aqr (Hollis & Koupelis 2000). The combination of collimated, “knotty,” X-ray emitting outflows and compact, central X-ray source observed in both Mz 3 and R Aqr is, morphologically, similar to that characteristic of AGNs (e.g., 3C 273, Marshall et al. 2001; Cen A, Hardcastle et al. 2003). In the case of the symbiotic Mira systems — as in AGNs — a natural relation between the X-ray-emitting core and jet(s) would be that the central engine has a mixture of closed small scale and open large scale fields, dynamically reforming. The jets flow along open field lines, while the point-like X-ray emission is generated via the dissipation of the closed structures as they

open, much like solar flares. This suggests that the core X-ray emission in Mz 3 and R Aqr may be variable; sensitive X-ray monitoring of these nebulae (and of NGC 6543, the other known example of both diffuse and point-like X-ray emission in a PN) is required to establish whether or not this is the case.

We caution that it remains to establish theoretically, via detailed numerical modeling, whether magnetic fields necessarily play a central role in either the launching or the collimation of jet-like outflows from evolved star systems. Nonetheless, the presence of compact X-ray sources and the appearance of X-ray emission that is confined to the outflow axes of the symbiotic Mira systems Mz 3 and R Aqr supports models that invoke collimating circumstellar disks driving high-velocity jets to explain the profound bipolar structure of these and other, similar nebulae around evolved stars.

Support for this research was provided by NASA/CXO grant GO2–3009X to RIT. Geoffrey Franz assisted in preparation of data for Figs. 1 and 3. N.S. acknowledges support from the US-Israel Binational Science Foundation. S.D.V acknowledges support from NASA grant NAG5–6711.

## REFERENCES

- Balick, B., & Frank, A. 2002, *ARA&A*, 40, 439
- Blackman, E.G., Frank, A., Markiel, J.A., Thomas, J.H., & Van Horn, H.M. 2001a, *Nature*, 409, 485
- Blackman, E.G., Frank, A., & Welch, C. 2001b, *ApJ*, 546, 288
- Bujarrabal, V., Castro-Carrizo, A., Alcolea, J., & Sánchez-Contreras, C. 2001, *A&A*, 377, 868
- Cassinelli, J. P., Cohen, D. H., MacFarlane, J. J., Sanders, W. T., & Welsh, B. Y. 1994, *ApJ*, 421, 705
- Chu, Y.-H., Guerrero, M.A., Gruendl, R.A., Williams, R.M., & Kaler, J.B. 2001, *ApJ*, 553, L69
- Ferrari, A. 1998, *ARA&A*, 36, 539
- Frank, A., Blackman, E., Gardiner, G., & Lery, T. 2003, *ApJ*, submitted
- García-Segura, G., López, J. A., & Franco, J. 2003, *RMxAC*, 15, 12
- Guerrero, M.A., Chu, Y.-H., Gruendl, R.A., Williams, R.M., & Kaler, J.B. 2001, *ApJ*, 553, L55



- Guerrero, M.A., Gruendl, R.A., & Chu, Y.-H. 2002, *A&A*, 387, L1
- Guerrero, M.A., Miranda, L.F., & Chu, Y.-H. 2003, *BAAS* 201, 89.09
- Hardcastle, M. J., Worrall, D. M., Kraft, R. P., Forman, W. R., Jones, C., & Murray, S. S. 2003, *ApJ*, in press (astro-ph/0304443)
- Hollis, J. M., & Koupelis, T. 2000, *ApJ*, 528, 418
- Kastner, J.H., Soker, N., & Rappaport, S.A., eds. 2000a, *Asymmetrical Planetary Nebulae II: from Origins to Microstructures*, *Astron. Soc. Pac. Conf. Ser.*, Vol. 199
- Kastner, J.H., Soker, N., Vrřílek, S.D., & Dgani, R. 2000b, *ApJ*, 545, L57
- Kastner, J.H., Vrřílek, S.D., & Soker, N. 2001, *ApJ*, 550, L189
- Kastner, J.H., Li, J., Vrřílek, S.D., Gatley, I., Merrill, K.M., & Soker, N. 2002, *ApJ*, 581, 1225
- Kellogg, E., Pedelty, J.A., & Lyon, R.G., *ApJ*, 563, L151
- Kingsburgh, R.L., & English, J., 1992, *MNRAS*, 259, 635
- Li, J., Kastner, J.H., Prigozhin, G., & Schulz, N.S. 2003, *ApJ*, in press
- López, J.A., & Meaburn, J. 1983, *MNRAS*, 204, 203
- Maness, H., Vrřílek, S.D., Soker, N., & Kastner, J.H. 2003, *ApJ*, in press
- Marshall, H.L., et al. 2001, *ApJ*, 549, L167
- Mastrodemos, N., & Morris, M. 1999, *ApJ*, 523, 357
- O’Dwyer, I. J., Chu, Y.-H., Gruendl, R. A., Guerrero, M. A., & Webbink, R. F. 2003, *AJ*, 125, 2239
- Pravdo, S. H., Feigelson, E. D., Garmire, G., Maeda, Y., Tsuboi, Y., & Bally, J. 2001, *Nature*, 413, 708
- Pudritz, R. E. & Konigl, A. 2000, in *Protostars & Planets IV*, eds. V. Mannings, A. P. Boss, and S. S. Russell (Univ. of Arizona Press), 759
- Redman, M.P., O’Connor, J.A., Holloway, J.A., Bryce, M., & Meaburn, J. 2000, *MNRAS*, 312, L23
- Reyes-Ruiz, M., & López, J.A. 1999, *ApJ*, 524, 952
- Sahai, R., & Trauger, J. 1998, *AJ*, 116, 1357
- Schmeja, S., & Kimeswenger, S. 2001, *A&*, 377, L18
- Soker, N., & Kastner, J.H. 2002, *ApJ*, 570, 245
- Soker, N., & Kastner, J.H. 2003a, *ApJ*, 583, 368

Soker, N., & Kastner, J.H. 2003b, ApJ, in press

Soker, N., & Rappaport, S. 2000, ApJ, 538, 241

Zhang, Y., & Liu, X.-W. 2002, MNRAS, 337, 499

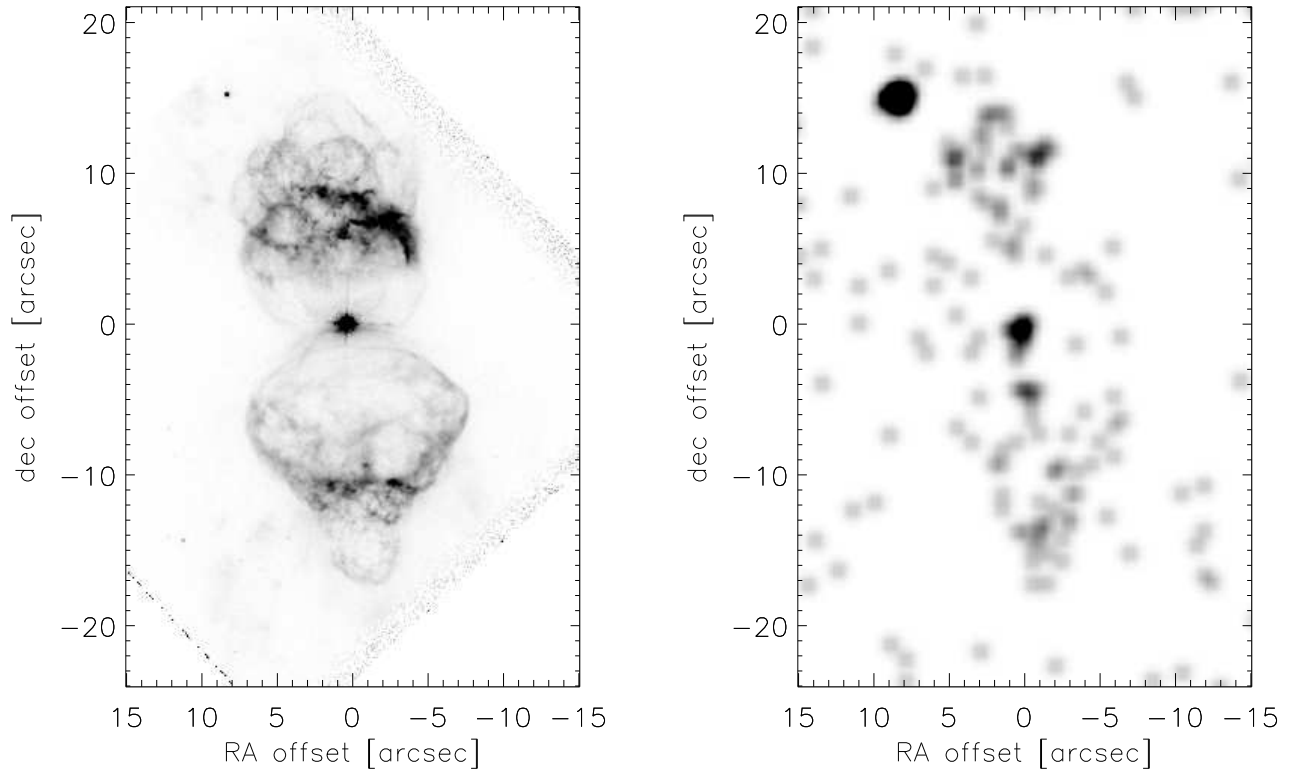


Fig. 1.— Comparison of HST visual-wavelength ( $H\alpha$ ; left) and Chandra/ACIS-S3 X-ray (right) images of Menzel 3. The X-ray image is constructed for the energy range 0.7 to 2.0 keV.

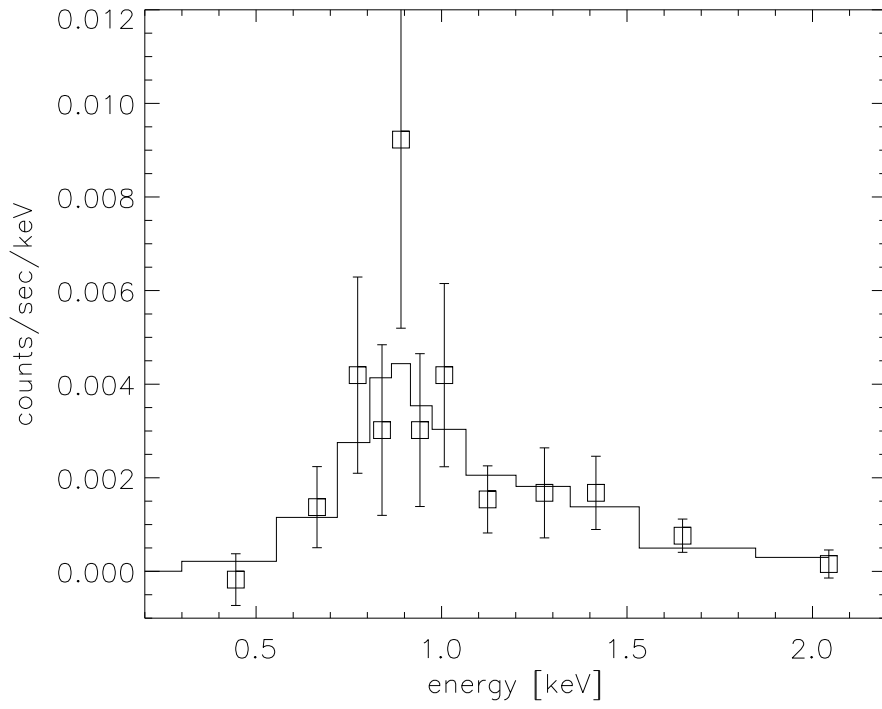


Fig. 2.— ACIS-S3 spectrum of Menzel 3 (squares), with best-fit absorbed VMEKAL emission model (histogram) overlaid.

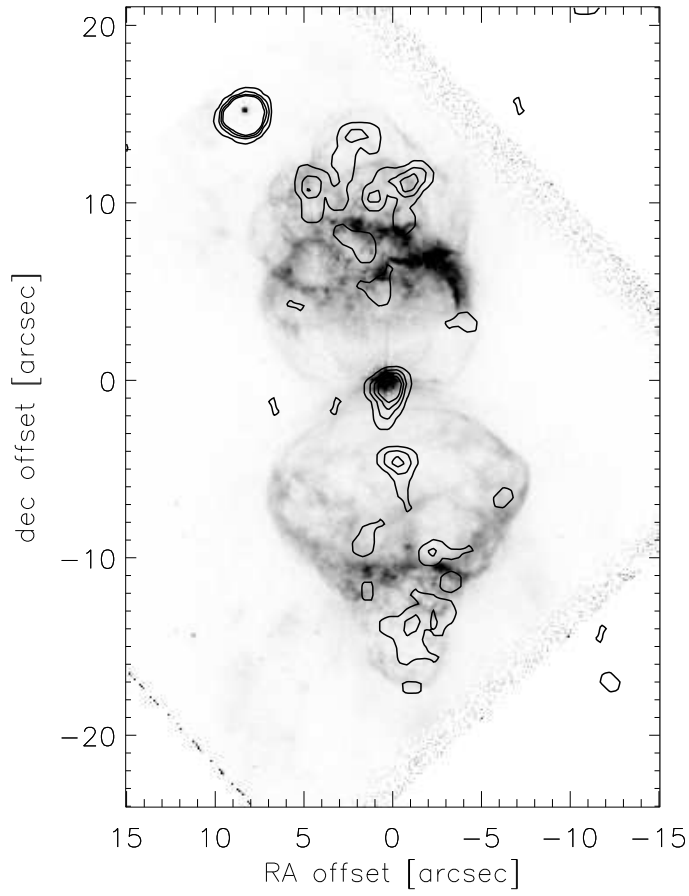


Fig. 3.— HST H $\alpha$  image of Menzel 3, with contour plot of Chandra/ACIS-S3 image overlaid. Contours are at levels of 1.0, 2.0, 3.0, and 4.0 counts pixel<sup>-1</sup>.